Nonlinear Dynamics of a VOC Combustion Loop Reactor

Pietro Altimari, Pier Luca Maffettone, and Silvestro Crescitelli
Dipartimento d'Ingegneria Chimica Università "Federico II" Piazzale Tecchio 80,80125 Napoli, Italy

Lucia Russo
Dipartimento di Ingegneria Chimica Alimentare Università di Salerno, Via Ponte Don Melillo, 84084, Fisciano (SA), Italy

Erasmo Mancusi
Facoltà di Ingegneria, Università del Sannio, Piazza Roma, 82100, Benevento, Italy

DOI 10.1002/aic.10878
Published online May 12, 2006 in Wiley InterScience (www.interscience.wiley.com).

Bifurcation analysis of a network of three catalytic combustors with periodically switched feed position is carried out. The influence of the switch time, of the feed temperature and of the heat exchange coefficient at the wall on the dynamical behavior is studied by a numerical continuation technique based on the spatiotemporal symmetry of the forced system. Symmetric and asymmetric periodic regimes are detected as the bifurcation parameters are changed. The stability range of periodic ignited regimes and their bifurcations are analyzed. In particular, it appears that some complex regimes are the only stable ignited regimes at ambient feed temperature in several operating conditions. © 2006 American Institute of Chemical Engineers *AIChE J,* 52: 2812–2822, 2006
Keywords: loop reactors, nonlinear dynamics, symmetric dynamical systems, periodically forced chemical reactors, bifurcation analysis

Introduction

Autothermal catalytic combustion in packed beds is often used to decontaminate polluted volatile organic compounds (VOCs) (see for a review Kolios et al.[1]). Catalytic combustion requires relatively high-temperatures of the catalytic bed, and, thus, feed preheating is needed: the cold, fresh, gaseous feed stream is preheated by the hot, exhausted, outlet gases in an external heat exchanger. However, this technique becomes exceedingly expensive for very low-fuel load, and, in some cases, unaffordable.

Several studies have shown that autothermal catalytic combustion can be efficiently carried out in periodically forced reactors,[2] as for example in reverse flow reactors (RFRs). The RFR operation was originally suggested by Cottrell[3] as an efficient way to process dilute pollutant mixtures having low-adiabatic temperature rises. Indeed, experimental and theoretical studies have shown that a significant improvement of energetic costs is obtained for catalytic combustion of lean VOCs mixtures by exploiting the high-heat capacity of catalytic fixed-bed reactors.[4-8] Stable dynamic regimes are obtained by periodically inverting the flow direction.[9, 10] In such a way, after an initial transient, a bell shaped temperature profile is obtained, which moves inside the reactor in a periodic fashion, trapped by the reversing of flow: In such a way, cold and very lean VOC mixtures can be conveniently processed.

RFRs have proven to be cost-effective also for other catalytic processes. For example, the temperature decrease at both reactor exits typical of RFRs make these reactors useful to improve the yield of equilibrium-limited exothermic reactions (for example, methanol synthesis;[11-13] ammonia synthesis;[14, 15] sulfur dioxide oxidation[9, 16]).

An intrinsic disadvantage of RFRs is the washout effect: immediately upon flow reversal, a fraction of reactants is lost at the end of each cycle. To overcome this problem, Matros[14] has explored several configurations capable of inducing stable dynamic regimes. Washout problems was analyzed by Vanden Bussche and Froment[17], who proposed as a remedy the "star" reactor configuration. Networks of two or more catalytic beds reactors are one of most promising alternative to overcome washout problems.[14, 18, 19] In such a configuration, the dynamic regime is reached by periodically varying the feed position ac-

Correspondence concerning this artricle should be addressed to E. Mancusi at mancusi@unisannio.it.

cording to a cyclic permutation of the reactor sequence. In efficient operating conditions, the heat front propagates in a virtually closed loop while keeping constant the flow direction in each reactor. Haynes and Caram[18] and Fissore and Barresi[20] compared reverse flow reactors and networks for catalytic combustion. They pointed out that, in the operating conditions they chose, not only washout is drastically reduced, but also catalyst results to be more uniformly used in the network configuration. Both articles, however, show that in the case of networks, the range of switch times where periodic regimes are stable is very narrow.

Recently, in a very interesting analysis Sheintuch and Nekhamkina[21, 22] derived two limiting models for loop reactors, one obtained for very fast switch, and the other for infinite number of reactors. Their numerical simulations are based on a pseudohomogeneous one-dimensional (1-D) model of an adiabatic catalytic-bed reactor in which a generic irreversible exothermic reaction occurs. A theoretical analysis to determine the range of *T*-periodic regimes (there called pulse rotating waves[21, 22]) is also presented. Their analytical criteria is based on the thermal front velocity for adiabatic catalytic reactors described with pseudohomogeneous models proposed by Burghardt et al.[23]. Sheintuch and Nekhamkina[22] also showed with numerical simulations that by increasing the number of the loop units the results approach those obtained with the limiting model for an infinite number of units.

A pseudohomogeneous model, however, may be not able to capture the dynamics of catalytic forced reactors.[24] Furthermore, for small number of units and intermediate switch velocity, the dynamics of loop reactors can be much more complex:[22,25,26] in addition to simple periodic regimes with period equal to the forcing period, multiperiodic, quasi-periodic and even chaotic regimes can be found. The presence of such complex regimes are mainly due to Neimark-Sacker bifurcations and frequency locking phenomena, that are very common in periodically forced systems, where the natural and forcing frequency interact.[26-29]

The knowledge of all possible regimes when the relevant design and operation parameters are changed is required to properly design and control periodically forced reactors. Bifurcation analysis is then the natural tool to investigate their dynamics, as it proves to be particularly useful for identifying multistability regions (for example, [30-32]).

An efficient methodology for bifurcation analysis with parameter continuation of periodically forced networks consisting of identical lumped parameters reactors was proposed by Russo et al.[33] This methodology, that was recently also applied to distributed parameters reactors,[26] is based on the spatiotemporal symmetry properties of those systems, and on the use of a nonstroboscopic map. This technique is completely general and independent by the number of reactors of the loop, and it applies to a wide class of reactor systems that exhibit the symmetry $Z_n \times S^1$, the symmetry depending only on the periodic forcing.[33]

In this article, we exploit this approach to study the nonlinear dynamics of a forced network of three fixed-bed reactors modeled as heterogeneous distributed parameter systems where catalytic combustion of VOCs takes place. In particular, we characterize, through bifurcation analysis, the stability domain of periodic regimes when the switch time, the feed temperature and the heat-transfer coefficient at the wall are changed.

Mathematical model

A variety of mathematical models with different level of complexity is available from the literature to describe the dynamics of fixed-bed reactors (for example, Froment and Bischoff[34]). Two classes of 1-D-models are commonly adopted: pseudohomogeneous models, which assume the same concentration and temperature for both solid and fluid phases that are treated as a single phase with properly averaged properties, and heterogeneous models, which account separately for mass and energy balances in both phases. When the temperature differences between the two phases are small, the predictions of both models are very close. In such a case, the simpler pseudohomogeneous description should be preferred. Some care should be paid, however, when the reactor is periodically forced. Indeed, simulations and bifurcation analysis performed by Khinast et al.[24] indicate that the pseudohomogeneous and the heterogeneous models for a RFR can predict different dynamic behaviors even when under steady operations the two-model give similar predictions. The difference emerges when the periodic forcing enhances temperature gradients between the phases. Moreover, for loop reactors differences are expected on the front velocity, and on the stability as suggested by Sheintuch and Nekhamkina[22].

In this work, in view of the importance of the possible differences between the phases, each fixed-bed reactor of the loop is modeled as a heterogeneous system. It is assumed that the fuel reacts following a first-order kinetics.[24] A similar model was implemented by Řeháček et al.[35, 36] for analyzing the dynamics of a reverse-flow reactor, but in this work a pseudo steady-state hypothesis for mass balance in the solid phase is assumed.

The following mathematical model for each catalytic reactor is then used

$$\begin{cases} \dfrac{\partial y_{g,i}}{\partial t} = \dfrac{1}{Pe_g^m}\dfrac{\partial^2 y_{g,i}}{\partial z^2} - \dfrac{\partial y_{g,i}}{\partial z} + J_g^m(y_{s,i} - y_{g,i}) \\ \dfrac{\partial \theta_{g,i}}{\partial t} = \dfrac{1}{Pe_g^h}\dfrac{\partial^2 \theta_{g,i}}{\partial z^2} - \dfrac{\partial \theta_{g,i}}{\partial z} + J_g^h(\theta_{s,i} - \theta_{g,i}) - \phi(\theta_{g,i} - \theta_{w,i}) \\ \dfrac{\partial \theta_{s,i}}{\partial t} = \dfrac{1}{Pe_s^h}\dfrac{\partial^2 \theta_{s,i}}{\partial z^2} - J_s^h(\theta_{s,i} - \theta_{g,i}) + B\eta Da(1 - y_{s,i})\exp\dfrac{\theta_{s,i}}{1 + \theta_{s,i}/\tilde{\gamma}} \\ J_s^m(y_{s,i} - y_{g,i}) = \eta Da(1 - y_{s,i})\exp\dfrac{\theta_{s,i}}{1 + \theta_{s,i}/\tilde{\gamma}} \end{cases} \quad i = 1, 2, 3 \tag{1}$$

In Eq. 1 the index i identifies the reactor. All the symbols are explained in the Notation.

The following boundary conditions for concentration in the gas phase and temperature in the solid and gas phases are assumed

$$\begin{cases} \left.\dfrac{\partial y_{g,i}}{\partial z}\right|_0 = -[1 - f(t-(i-1)\tau)]y_{in} - f(t-(i-1)\tau)y_{g,i-1}(1,t) + y_{g,i}(0,t) \\ \left.\dfrac{\partial \theta_{g,i}}{\partial z}\right|_0 = -[1 - f(t-(i-1)\tau)]\theta_{in} - f(t-(i-1)\tau)\theta_{g,i-1}(1,t) + \theta_{g,i}(0,t) \\ \left.\dfrac{\partial \theta_{s,i}}{\partial z}\right|_0 = 0 \end{cases} \tag{2}$$

$$\left.\frac{\partial y_{g,i}}{\partial z}\right|_1 = \left.\frac{\partial \theta_{g,i}}{\partial z}\right|_1 = \left.\frac{\partial \theta_{s,i}}{\partial z}\right|_1 = 0 \tag{3}$$

In Eqs. 1–3, the same nomenclature and dimensionless parameters of Řeháček et al.[35] have been adopted. As illustrated in Figure 1, the function *f(t)* is a square wave that accounts for the discontinuous feed scheme with τ as the switch time. The reactors are fed according to the sequence 1-2-3 in the time range $[0,\tau]$; after the first switch, that is in the range $[\tau,2\tau]$, they are fed according to the sequence 2-3-1; then, after the second switch ($t \in [2\tau, 3\tau[$), the reactors are fed as the sequence 3-1-2; the next switch brings the feed sequence to the first one, that is, 1-2-3, and the permutation cycle restarts (see Figure1).

It is apparent that the vector field changes discontinuously in time, and it recovers the same form after a time $T = 3\tau$. Indeed, *f(t)* is a discontinuous periodic function with minimum period T, and the nonautonomous system 1-3 is, thus, T periodic.

The reactor model (Eqs. 1–3) can be written in abstract form as the following dynamical system

$$\begin{cases} \dot{\mathbf{x}} = \mathbf{F}(\mathbf{x}, \boldsymbol{\lambda}, t) \quad \mathbf{F}(\mathbf{x}, \boldsymbol{\lambda}, t) = \mathbf{F}(\mathbf{x}, \boldsymbol{\lambda}, t+T) \\ \mathbf{x}(t_0) = \mathbf{x}_0 \end{cases} \tag{4}$$

In Eq. 4, $\mathbf{x} \equiv (\mathbf{x}_1(z,t), \mathbf{x}_2(z,t), \mathbf{x}_3(z,t))$ is the state vector of the system, $\mathbf{x}_i \equiv (y_{g,i}(z,t), \theta_{g,i}(z,t), \theta_{s,i}(z,t))$ is the state vector of each reactor, and $\boldsymbol{\lambda} \equiv (\tau, Pe_g^m, J_g^m, Pe_g^h, J_g^h, \phi, J_s^m, Da, Pe_s^h, J_s^h, B, \tilde{\gamma})$ is the parameter vector.

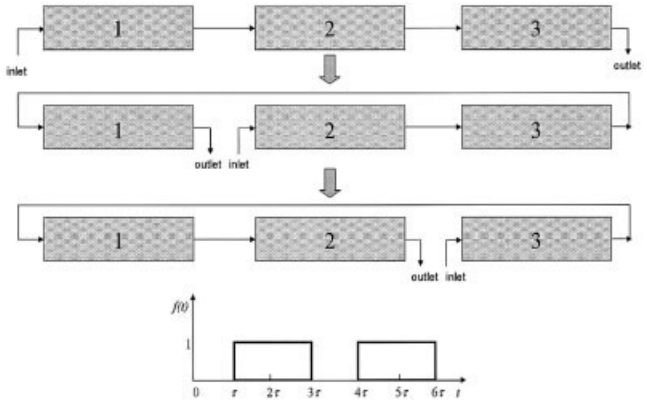

Figure 1. Three catalytic reactors with variable feed and discharge positions.

The forcing function *f(t)* appearing in Eq. (2) is also reported.

Results

The spatiotemporal patterns predicted as parameters are changed are classified by making use of symmetry properties of the model and bifurcation theory. This section is structured as follows. First, symmetry properties of reactor models and of spatiotemporal patterns are discussed. Then, we report a detailed analysis of the local bifurcations encountered when the switch time is varied for a fixed-feed temperature value. Next, the influence of the inlet temperature on the network dynamics for different switch times is addressed. Hysteretic phenomena and multistability are detected and discussed. Finally, the influence on the dynamics of the heat-transfer coefficient at the wall is examined.

All the parameter values that are kept constant throughout the article are reported in Table I.

Symmetry Properties

The loop reactor under investigation is a T-periodic discontinuous system, and, thus, fundamental regimes are T-periodic solutions, which manifest as periodic spatiotemporal patterns for the distributed nature of the model. Invariance properties can be easily recognized from the analysis of the evolution profiles in each reactor. An example of a spatiotemporal pattern corresponding to a T-periodic regime is reported in Figure 2.

In Figure 2, each box corresponds to a different reactor, the horizontal coordinate is the dimensionless axial position, and the vertical coordinate is the time made nondimensional through the switch time. The correspondence between the level of concentration and temperatures and the gray scale is reported in the figure legend. During the first time interval $0 < t < 1$, the reactor 1 is fed with fresh reactant and the output stream exits from reactor 3. The temperature front forms in the first reactor, and then moves along axially. According to the forcing policy, after the first switch, a new front forms and moves along the second reactor, then after the second switch the same happens in the third reactor. From a global point of view, this means that the profiles in each reactor at time t are simply shifted to the next reactor at time $t+\tau$. Namely, the following relation holds

$$\mathbf{x}_1(z,t) = \mathbf{x}_2(z, t+\tau) = \mathbf{x}_3(z, t+2\tau). \tag{5}$$

Table 1. Parameter Values in Eqs. 1–3

$Da = Lr_{in}/(\nu\varepsilon_s)$	Damköler number	0.32
η	Effectiveness factor of the catalyst	1.
$\tilde{\gamma} = E/(RT_0^*)$	Nondimensional activation energy	16.68
$Pe_g^m = L\nu/D$	Péclet number for mass in gas phase	105.82
$Pe_g^h = \rho_g c_{pg} L\nu/k_g$	Péclet number for energy in gas phase	214.66
$Pe_s^h = \rho_s c_{ps} L\nu/k_s$	Péclet number for energy in solid phase	$0.48\ 10^5$
$Le = (\rho_g c_{pg}\varepsilon + (1-\varepsilon)\rho_s c_{ps})/\rho_g c_{pg}\varepsilon$	Lewis number	1281
$J_g^m = k_m aL/(\nu\varepsilon)$	Nondimensional mass transfer coefficient	5.67
$J_s^m = k_m aL/(\nu\varepsilon_s(1-\varepsilon))$	Nondimensional mass transfer coefficient	7.63
$J_g^h = h_{fc} aL/(\rho_g c_{pg}\nu\varepsilon)$	Nondimensional heat transfer coefficient	9.46
$J_s^h = h_{fc} aL/(\rho_s c_{ps}\nu(1-\varepsilon))$	Nondimensional heat transfer coefficient	$7.5\ \ 10^{-3}$
$B = \Delta H C_{A,in}\gamma/(\rho_g c_{pg} T_0^*)$	Nondimensional adiabatic temperature increase	0.0097
θ_{in}	Nondimensional inlet gas temperature	−3.5
$y_{g,in}$	Nondimensional inlet conversion	0.
$\theta_w = (T_w^* - T_0^*)\gamma/T_0^*$	Nondimensional wall temperature	−9.6
$\phi = 4h_{fw}L/(\rho_g c_{pg} d_r \nu\varepsilon)$	Nondimensional heat transfer coefficient at the wall	0.24

Characteristic values of variables: inlet concentration $C_{in} = 0.003$ kmol/m^3, $\nu = 2$ m/s, L = 0.17 m and a $T_0 = 730$ K (Řeháček et al.[35]).

Thus, this regime is a discrete traveling (or rotating) wave, or, more picturesquely, a *ponies on merry-go-round* solutions.[37] It should be noted that Sheintuch and Nekhamkina[22] call these solutions "rotating-pulse solutions". It can be easily verified that the property expressed in Eq. 5 is due to the spatiotemporal symmetry of the periodic regime. Indeed, with G the linear operator that takes into account the permutation order of the reactors

$$G\mathbf{x}(z,t) = \begin{pmatrix} 0 & I & 0 \\ 0 & 0 & I \\ I & 0 & 0 \end{pmatrix} \begin{pmatrix} \mathbf{x}_1(z,t) \\ \mathbf{x}_2(z,t) \\ \mathbf{x}_3(z,t) \end{pmatrix} = \begin{pmatrix} \mathbf{x}_2(z,t) \\ \mathbf{x}_3(z,t) \\ \mathbf{x}_1(z,t) \end{pmatrix} \tag{6}$$

where I is the identity operator ($I\mathbf{x}_i = \mathbf{x}_i$), the following invariance property holds true

$$\mathbf{x}(z,t) = G\mathbf{x}(z, t+\tau) \tag{7}$$

Of course, the invariance property in Eq. 7 can be generalized to a generic number, N, of reactors. Equation 7 generalizes a result of Swift and Wiesenfeld[38]. The presence of spatiotemporal symmetry in the solutions of the dynamical system given by the Eq. 4 is strictly connected to the periodic forcing. Indeed, the periodic discontinuous forcing introduces symmetry in this dynamical system even when the unforced system would not possess any spatial symmetry as demonstrated by Russo et al.[26, 33] In the case under investigation, this spatiotemporal symmetry obeys the following invariance property

$$G\mathbf{F}(\mathbf{x}, \boldsymbol{\lambda}, t) = \mathbf{F}(G\mathbf{x}, \boldsymbol{\lambda}, t-\tau) \tag{8}$$

As the equality $G^3 = I$ holds true, G is the generator of a spatial symmetry group isomorphic to the cyclic group Z_3.[39] A relation similar to Eq. 8 also holds for G^2, the time shift being in such a case 2τ. Details on the spatiotemporal symmetry of the system can be found in Russo et al.[26, 33] Despite the symmetry of the model equations, also asymmetric regimes may be found. For the asymmetric regimes, the Eq. 5 does not hold true, therefore, each reactor experiences a different time history. It is worth noting that in this case a multiplicity of G-conjugate asymmetric regimes is forced by the symmetry properties of the model and their selection depends on the choice of the initial conditions.[33] Examples of spatiotemporal patterns of three coexisting G-conjugate asymmetric $2T$-periodic regimes are reported in Figure 3a,b,c, respectively. The G relationship among the three reported regimes is apparent.

Furthermore, if we focus our attention on the regime re-

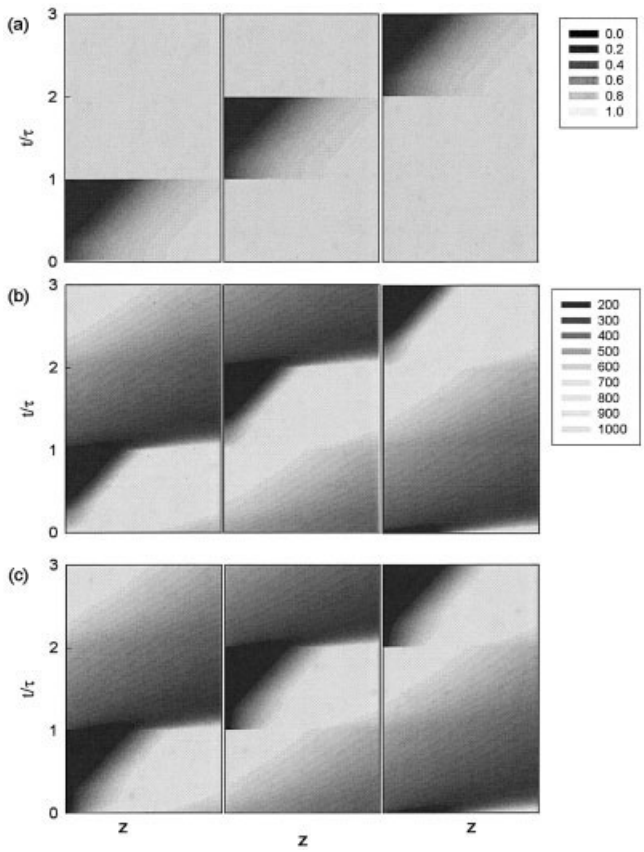

Figure 2. Spatiotemporal patterns of the (a) gas phase conversion, (b) solid phase temperature and (c) gas phase temperature for τ = 4,000, T_{in}= 240 C and ϕ = 0.24. Each box corresponds to a reactor unit.

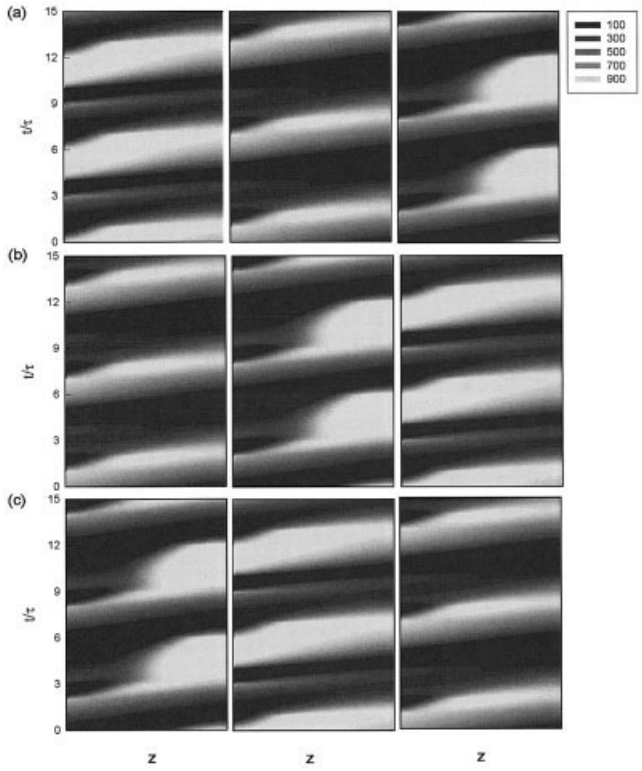

Figure 3. Spatiotemporal patterns of the temperature in the gas phase of three coexisting *G*-conjugate 2*T*-periodic regimes for τ = 1,000, T_{in} = 100 C and ϕ= 0.24.

Each box corresponds to a reactor unit.

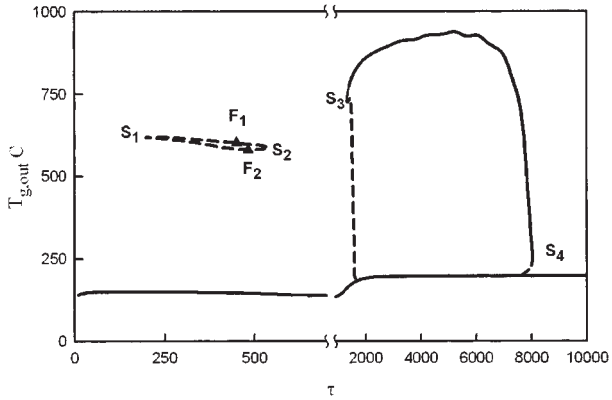

Figure 4. Symmetric *T*-periodic solution diagram with the switch time, τ, as bifurcation parameter for T_{in} = 240 C and ϕ = 0.24.

The solution is reported with the gas temperature at the network exit, C. Solid lines: stable *T*-periodic regimes; dashed lines: unstable *T*-periodic regimes; Fold bifurcations are indicated with the letter S, Flip bifurcations are indicated with the letter F and filled triangles.

ported in Figure 3a, reactors 1 and 3 appear thermally more stressed than reactor 2, as, there, higher-temperatures are experienced on the average. Hence, VOCs oxidation takes preferentially place in reactors 1 and 3 rather than the reactor 2, and the catalyst is not uniformly exploited. Of course, similar considerations can be done for the other two G-conjugate regimes reported in Figure 3b and c. It should be emphasized that strongly nonuniform catalyst utilization is the rule and not the exception when attaining asymmetric regimes. Indeed, since in such a case the three reactors experience different thermal histories, higher temperatures have to be expected in some reactors with respect to others. Symmetry breaking bifurcations leading to local temperature rises could of course have negative effects on catalyst activity and, hence, should be adequately prevented. The analysis of the symmetry properties of the reactor network provides useful guidelines when designing a robust control system. A rather obvious implication, for example, is that temperature sensors have to be placed in at least two different reactors in order to detect the onset of symmetry breaking. The possible nonuniform use of the catalyst in the presence of asymmetry suggests to reconsider the comparison between network of reactors and reverse flow reactor,[20] as the conclusion that a network of reactors determines a more uniform catalyst use with respect to the reverse flow configuration is correct only in the case of symmetric regime.

A systematic and accurate analysis of the symmetry breaking phenomena can be carried out through bifurcation analysis and parameter continuation. The bifurcation analysis can be conducted as proposed in[33] with application of pseudoarchlength continuation methods to numerically calculated Poincaré map, *P*. This technique is here used to obtain solution diagrams of symmetric *T*-periodic regimes.

Influence of the switch time τ

The switch time is an important operating parameter as a proper forcing may induce reactor ignition, and it can be used as manipulated variable in a control law.[40] Numerical simulations showed its relevance in both design and operation.[19] Thus, the knowledge of the bifurcation behavior of the reactor network as the switch time is varied is of value as it allows a quick and complete characterization of reactor performances in terms of ignition and switch off.

The regime solution diagram shown in Figure 4 presents the influence of the switch time on network dynamics. Stable and unstable *T*-periodic symmetric regimes are reported in Figure 4. The feed temperature value is fixed at 240 C. It should be noted that at this value of the feed temperature the unforced system does not exhibit stable ignited regimes. Solid lines in Figure 4 represent stable *T*-periodic regime, whereas dashed lines refer to unstable regimes. Filled triangles are used for Flip bifurcations (F_1 and F_2) and Saddle-Node bifurcations are indicated with letter S. Values of the switch time τ at the bifurcation points are reported in Table 2.

Table 2. Switch Time Values τ at the Bifurcation Points shown in Figure 4

	τ
S_1	197
S_2	536
S_3	1326
S_4	8030
F_1	450
F_2	482

It is apparent from Figure 4 that the switch time has a profound effect on the loop-reactor performances. In particular, two ranges characterized by different features and dynamical behaviors are detected. Two disconnected isolae of symmetric *T*-periodic regimes are found when the switch time is varied. At high τ-values, two catastrophic saddle-node bifurcation points S_3 and S_4, delimitate an isola of symmetric *T*-periodic regimes (note that the lower branch of the isola is barely distinguishable from the nonignited branch). *T*-periodic high-conversion regimes corresponding to the upper branch of the isola are stable, and coexist with stable nonignited regimes. Hence, the loop reactor is ignited for $\tau_{S3} < \tau < \tau_{S4}$, but for $\tau > \tau_{S4}$ the forcing is not able to sustain autothermal VOCs oxidation. Stable high conversion *T*-periodic regimes attained for $\tau \in [1326, 8030]$ are characterized by thermal and conversion fronts traveling along the loop reactor.

The limiting conditions for ignition, τ_{S3} and τ_{S4}, deserve some comments for their importance in operations. Analytic criteria for these two critical conditions were proposed by Sheintuch and Nekhamkina[22]. These criteria are based on a theoretical prediction of the front velocity[23] within pseudohomogeneous assumption and adiabatic operations. The predicted lower value, τ_{S3}, is the reciprocal of the ratio between effective and solid heat capacities (called *Le* in [22, 23]). The value here determined through bifurcation analysis for τ_{S3} (that is, the saddle-node bifurcation S_3) for the heterogeneous model is very close to the reciprocal of *Le* (1281) in agreement with the analytic prediction. The agreement is explained by considering that, the lower limit ($\tau = Le$ equivalently $V_{sw} = 1/Le$) represents the condition in which the switch velocity is equal to the maximum front velocity. It is obvious that the reactor network considered lives from moving an exothermic reaction front around. This implies that the feed switching must not be faster than the front movement to guarantee the propagation of a reaction front in the network. The maximum front moving velocity is that of a purely thermal front in packed beds. Therefore, a switch velocity greater than this value does not guarantee front formation. Obviously, this condition does not depend on the model (pseudohomogeneous or heterogeneous, adiabatic or nonadiabatic).

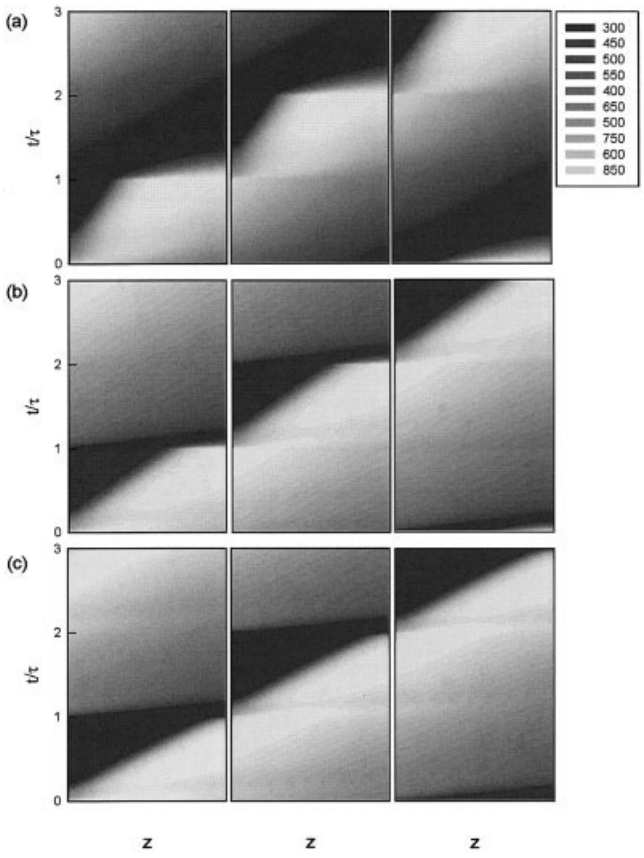

Figure 5. Spatio-temporal patterns of the temperature in the gas phase for (a) τ = 3,000, (b) τ = 6,000, and (c) τ = 8,000 T_{in} = 240 C, and ϕ = 0.24.

Each box corresponds to a reactor unit.

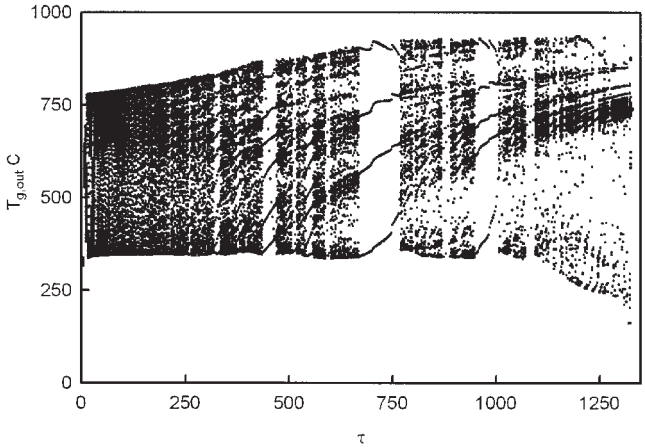

Figure 6. Asymptotic behavior for $\tau \in$ [20, 1326] T_{in} = 240 C and ϕ = 0.24.

The state is represented by the gas temperature at the at the exit of the NTW.

The saddle node bifurcation point S_4 corresponds to the condition in which the switch velocity V_{sw} reaches the front velocity V_{fr}.[22] Spatiotemporal patterns corresponding to symmetric regimes are shown in Figure 5 for increasing values of the switch time.

Symmetry of the *T*-periodic regimes are self evident, as the three reactors experience the same thermal histories. Thermal front velocities are readily evaluated as the slope of the line-boundary separating the cold region and the hot one. They are found to be unaffected by the switch time. Indeed, thermal waves invariably travel along the reactor network at the dimensionless velocity $V_{fr} \approx 2.5 \times 10^{-4}$ m/s. The spatiotemporal patterns become smoother and smoother as the switch time is increased. At the saddle-node bifurcation S_4 (τ_{S4} = 8030) the switch velocity V_{sw} reaches the front velocity V_{fr}, and for higher values of the switch time thermal front exits the reactor, thus, leading the reactor to shut-off.

At low-switch time values an isola of unstable symmetric *T*-periodic regimes delimitated by two saddle-node bifurcation points S_1 and S_2, is also found (Figure 4). No ignited, stable, *T*-periodic regime is found for $\tau < \tau_{S3}$. Nonetheless, complex ignited regimes are detected in this parameter range, persisting down to very low-switch time values. These solutions are determined via simulation, and their asymptotic behavior, which vary with the switch time, in the range $\tau \in [30, 1326]$ is reported in Figure 6. In

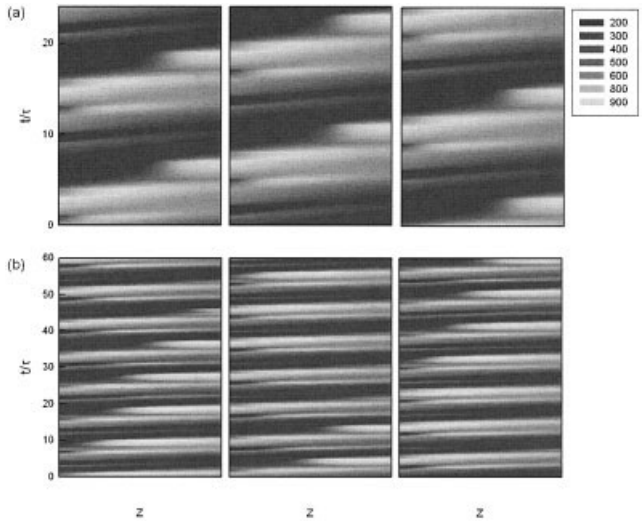

Figure 7. Spatiotemporal patterns of the temperature in the gas phase for T_{in} = 240 C and ϕ = 0.24.

(a) a 4*T*-periodic symmetric regime at τ = 900, and (b) a symmetric quasi-periodic regime at τ = 700. Each box corresponds to a reactor unit.

Figure 6, one thousand iterates of the Poincarè map after transients that have died out, are plotted for each τ-value.

It can be noted that for switch time values below the saddle-node bifurcation point S_3, "complex" ignited regimes are found. Therefore, the saddle-node bifurcation S_3 does not correspond to the extinction condition. In fact, as the switch time is decreased, quasi-periodic and multiperiodic ignited regimes are detected. Multiperiodic regimes are related to frequency-locking phenomena, a common feature in forced systems arising from the interaction between two frequencies, for example, the natural and the forcing frequencies.[27-29, 41] Indeed, quasi-periodic orbits evolve on an invariant T^2 torus, and are characterized by two frequencies that are in an irrational ratio.[32] As the switch time is changed, the forcing frequency varies, and may "lock" onto the natural frequency when their ratio becomes rational, so giving rise to a k*T*-periodic resonant regime with periodicity multiple of the forcing period. Multiperiodic windows become narrower and narrower as the switch time is further decreased, and eventually only quasi periodic regimes are found for switch time values lower than τ = 200.

By way of example, Figure 7 shows some complex spatiotemporal patterns found at switch times lower than τ_{S3}.

Figure 7a shows a spatiotemporal pattern of a 4*T*-periodic symmetric regime, while in Figure 7b a symmetric quasi-periodic pattern is reported. It is worth noting that in quasi-periodic condition, switch after switch, the ignition position *irregularly* changes, and it does not follow a regular periodic law anymore. Moreover, although these complex regimes correspond to ignited regimes, below τ_{S3} there is no time for the traveling front to form, and this is apparent from the spatiotemporal patterns (see Figure7). It should be noted that several multiperiodic regimes encountered for $\tau<\tau_{S3}$ are asymmetric. Indeed, frequency locking phenomena may induce symmetry breaking[26, 42].

A 2*T*-periodic asymmetric regime is reported in Figure 8. It is apparent that the asymmetric regimes are characterized by different spatiotemporal patterns for the three reactors. This implies, of course, that the average conversion and temperature in each reactor are not the same as in the case of symmetric regimes. The occurrence of a multiplicity of asymmetric regimes poses the obvious consequence that the loop reactor runs in nonuniform conditions, as each element of the network may experience a different history as already mentioned in the previous section.

The bifurcation scenario for $\tau<\tau_{S3}$ is very complex, and a detailed description of complex regime transitions like frequency locking phenomena, torus bifurcations and routes to chaos can be found elsewhere[26].

Influence of the inlet temperature T_{in}.

Another important parameter in design and operation is the feed temperature. During operations, this variable can experience significant variations in time possibly causing reactor shut off if a robust control strategy is not implemented. The influence of the feed temperature on the forced network dynamics is here considered first for $\tau < \tau_{S3} \sim Le$, then for $\tau \in [\tau_{S3}, \tau_{S4}]$ (see Figure 4). Solution diagrams of *T*-periodic symmetric regimes with the feed temperature as bifurcation parameter for four different switch time values in the range [1,500,6,000] are reported in Figure 9. Values of the inlet temperature at the bifurcation points are reported in Table 3.

For τ<4,000 (Figure 9a,b) a catastrophic saddle-node bifurcation point S_1 delimitates a wide inlet temperature range where coexistence of stable and unstable symmetric *T*-periodic regimes is predicted. Stable *T*-periodic high conversion regimes are found down to ambient temperature. For τ>4,000, a catastrophic saddle-node bifurcation point, S_2, is detected at inlet temperature values close to the ambient temperature (Figure 9c,d). This saddle-node bifurcation point marks the limit of ignited states, shut off occurring for lower inlet temperatures. The saddle-node bifurcation point S_2 shifts at larger inlet temperature values as the switch time is increased as shown in Figure10, where the locus of the saddle-node bifurcation (S_2) in the plane T_{in}-τ is reported. As the switch time is increased this locus asymptotically approaches the inlet temperature corresponding to the saddle-node S_2 ($\approx$280 C) calculated for the unforced network of three reactors. This trend is easily explained by considering that as the switch time is increased the

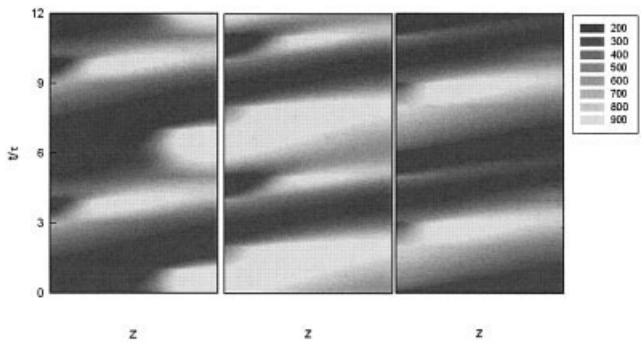

Figure 8. Spatiotemporal patterns of the temperature in the gas phase for a 2*T*-periodic asymmetric regime at τ= 1085, T_{in} = 240 C and ϕ = 0.24.

Each box corresponds to a reactor unit.

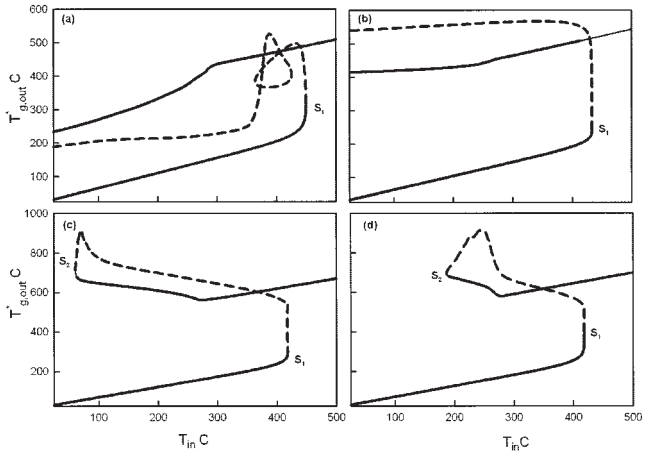

Figure 9. Symmetric *T*-periodic solution diagrams with T_{in} as the bifurcation parameter.

The solution is reported as the gas temperature at the end of the NTW. We use the same symbol defined in Figure 4. (a) $\tau = 1{,}500$; (b) $\tau = 2{,}000$; (c) $\tau = 4{,}000$, and (d) $\tau = 6{,}000$. In all the cases $\phi = 0.24$.

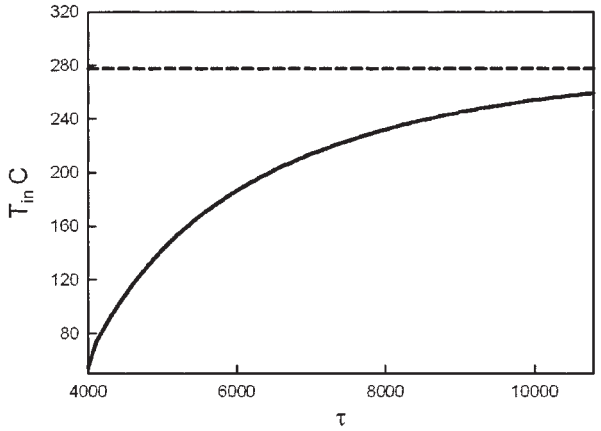

Figure 10. Bifurcation diagram in the plane T_{in}-τ for ϕ = 0.24.

Solid line is the bifurcation locus of bifurcation S_2 in Figure 9. Dashed line is the asymptotic behavior of the unforced network.

system tends to become similar to the unforced network, thus implying a more difficult ignition.

The inlet temperature values at the saddle-node S_2 are highly sensitive to the switch time. Hence, for $\tau \in [4000, 8000]$ the switch time can be conceived as a suitable manipulated variable to reject disturbances in the inlet temperature, and to avoid shut-off of the network.

As reported in the previous subsection, rich dynamics is observed at low-switch time values. In this range of switch time values, the feed temperature plays an important role on the bifurcation behavior of the network. Figure 11 shows the regime solution diagrams and the corresponding asymptotic behavior with T_{in} as the bifurcation parameter at four different switch time values ($\tau \in [50, 1000]$). Solution branches corresponding to *T*-periodic symmetric regimes, are reported in Figure 11a–d as the inlet temperature T_{in} is varied. The asymptotic behavior is reported in Figure 11e–h as the inlet temperature T_{in} is varied in the range [30, 400]. One thousand iterates of the Poincarè map, taken after transients have died out, are plotted for each T_{in}. All remaining parameters have been kept constant to the values reported in Table 1.

Values of the inlet temperature at the bifurcation points are reported in Table 4.

At low-feed temperatures, the only stable *T*-periodic symmetric regimes correspond to extinguished conditions. At larger values of the feed temperature, two saddle-node bifurcation points S_1 and S_2 delimitate a range of coexistence of three *T*-periodic symmetric regimes, that is, the reactor network invariably experiences a hysteresis. As the bifurcation parameter is further increased, high-conversion *T*-periodic regimes are predicted. It should be noted that this solution branch becomes stable at a Neimark-Sacker (N-S_1) bifurcation for all the switch time values investigated. Therefore, *T*-periodic symmetric regimes vanish in correspondence of the Neimark-Sacker bifurcation N-S_1. This bifurcation marks the onset of stable quasi-periodic regimes that extend toward low-inlet temperatures. The bifurcation scenario of *T*-periodic symmetric regimes, however, is only slightly affected by the investigated switch time values (see Table 4). Therefore, the stability range of high conversion *T*-periodic regimes does not change significantly as the switch time is increased in such a range.

Table 3. Values of the Inlet Temperature T_{in} at the Bifurcations Points shown in Figure 9 (a) $\in$ = 1,500; (b) $\in$ = 2,000; (c) $\in$ = 3,000; (d) $\in$ = 6,000

	T_{in} (a)
S_1	240.62
	T_{in} (b)
S_1	237.60
	T_{in} (c)
S_1	234.82
S_2	493.97
	T_{in} (d)
S_1	288.90
S_2	473.45

It is apparent from the asymptotic behaviors reported in Figures 11e-h that stable ignited complex regimes are predicted for $T_{in} < T^*_{in,S_1}$. In particular, coexistence of stable quasi-periodic or multiperiodic regimes with extinguished *T*-periodic regimes is found in a wide range of inlet temperatures close to the ambient temperature. As Neimark-Sacker bifurcations are symmetry preserving bifurcations[43,44], symmetry breaks through frequency locking phenomena (Figure11c,d,e,h). An example of a resonant asymmetric 2*T*-periodic regime for this value of parameters was shown in Figure 3.

The basins of attraction of these complex ignited attractors, and of the nonignited *T*-periodic attractors regimes are separated by the stable manifold of the saddle T^2 tori emerging from the Neimark-Sacker bifurcation point N-S_4. In such a switch time range, autothermal VOCs oxidation could be performed, even at very low-feed temperature, under quasi-periodic or multiperiodic conditions. It could also be noted that as the switch time is increased windows corresponding to frequency locking phenomena become progressively wider. Indeed, at the lowest switch time value (Figure 11e), the asymptotic behavior is quasi-periodic throughout the explored range. Conversely, at the largest switch time value (Figure 11h) only multiperiodic regimes are predicted.

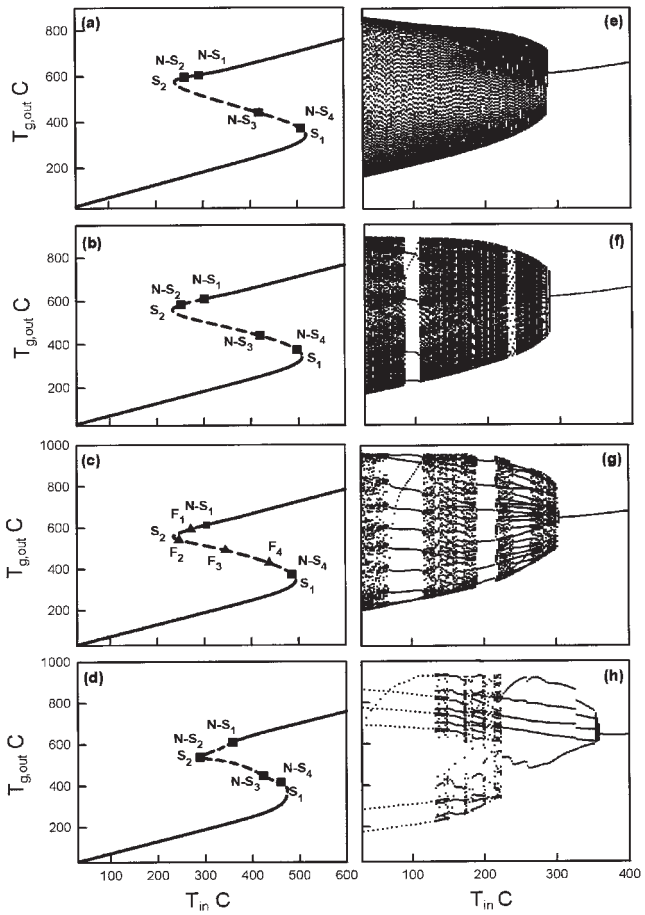

Figure 11. Symmetric *T*-periodic solution diagrams (on the left) and the asymptotic behavior (on the right) with T_{in} as the bifurcation parameter.

The solution is reported as the gas temperature at the end of the NTW. We use the same symbol defined in Figure 4. (a), (e) $\tau = 50$; (b), (f) $\tau = 300$; (c), (g) $\tau = 500$; (d), (h) $\tau = 1{,}000$. In all the cases $\phi = 0.24$.

The situation shown for low switch time values (Figure 11) is significantly different with respect to that found at higher switch time values (Figure 9). Indeed, at low switch time values the switch time does not affect significantly the minimum value of the inlet temperature ($T_{in\text{-}N\text{-}S1}$) for the ignition to occur in a stable *T*-periodic regime. Moreover, while in the case of high switch time values complex regimes are absent, they exist in a wide range of the inlet temperature for low switch times.

Influence of the heat-transfer coefficient ϕ

A cooling system can be used to avoid hot spot formations and catalyst overheating under process conditions, while for pilot scale reactors is very difficult to avoid heat losses. Therefore, it can be useful to know the effect of the heat losses on the dynamics of the loop of reactors.[45] This effect is here studied choosing the heat-transfer coefficient at the wall (ϕ) as a parameter which takes into account heat losses. In Figure 12 symmetric *T*-periodic regimes are displayed as the inlet temperature is varied for decreasing heat-transfer coefficient values, and for four different switch time values ($\tau < \tau_{S3} \sim Le$, see Figure 4).

Table 4. Values of the Inlet Temperature T_{in} at the Bifurcations Points shown in Figure 11 (a) $\in$ = 50; (b) $\in$ = 300; (c) $\in$ = 500; (d) $\in$ = 1,000

	T_{in} (a)		T_{in} (c)
S_1	519.14	S_1	493.97
S_2	240.62	S_2	234.82
N—S_1	290.96	N—S_1	305.25
N—S_2	261.53	N—S_2	486.52
N—S_3	418.92	F_1	217.94
N—S_4	508.14	F_2	245.45
		F_3	345.39
		F_4	437.55
	T_{in} (b)		T_{in} (d)
S_1	508.16	S_1	473.45
S_2	237.60	S_2	288.90
N—S_1	301.25	N—S_1	358.69
N—S_2	252.48	N—S_2	289.34
N—S_3	419.05	N—S_3	422.87
N—S_4	497.59	N—S_4	460.41

The bifurcation behavior of the network with respect to the inlet temperature is only quantitatively affected by changes of the heat-transfer coefficient at the wall. Indeed, as the inlet temperature is decreased, a hysteresis is always predicted, and high-conversion *T*-periodic regimes become unstable through Neimark-Sacker bifurcations. Nevertheless, as the heat transfer coefficient is decreased the Neimark-Sacker bifurcation point giving rise to the onset of ignited quasi-periodic regimes shifts at lower and lower T_{in} values, thus enlarging the range of stability of high conversion *T*-periodic regimes. However, for the set of parameters considered in this work, under adiabatic operating conditions this Neimark-Sacker bifurcation shifts to inlet temperature values that are not relevant from a practical point of view.

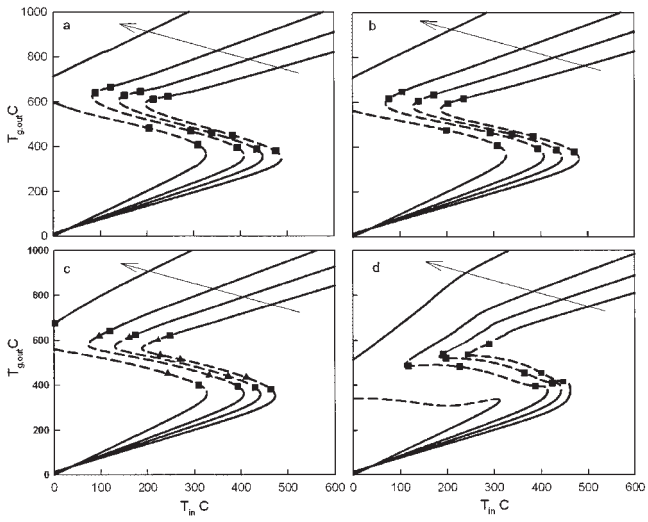

Figure 12. Symmetric *T*-periodic solution diagrams with T_{in} as the bifurcation parameter.

The solution is reported as the gas temperature at the end of the NTW. We use the same symbol defined in Figure 4. (a) $\tau = 50$; (b) $\tau = 300$; (c) $\tau = 500$; (d) $\tau = 1{,}000$. The arrows indicate the versus of the heat exchange coefficient decrease. Four values are considered: $\phi = 0.2$, $\phi = 0.15$, $\phi = 0.1$, and $\phi = 0$.

From other calculations here not reported for brevity, we observed that for switch time in the range $[\tau_{S3}, \tau_{S4}]$ (see Figure 4), and independently from the heat losses, there are not bifurcations leading to complex regimes. This feature is in agreement with Khinast et al.[45] where a RFR is studied. Indeed, Khinast et al.[45] showed in their Figure 7 that above a critical switch time (≈ 140) no complex bifurcation is found whatever the values of the cooling capacity.

Conclusion

In this work, the dynamics of a forced network of three catalytic combustors has been analyzed by considering the switch time, the feed temperature and the heat-transfer coefficient at the wall as bifurcation parameters. Each reactor in the network is modeled by an heterogeneous model as interphase gradients are important under forced conditions.[24] The complete bifurcation analysis reported is obtained through a continuation technique based on the spatiotemporal symmetries[33] of the network.

A first important conclusion refers to the possible occurrence of symmetric or asymmetric regimes. As clearly shown, the existence of asymmetric regimes implies that the three reactors of the loop experience different spatio-temporal patterns, and, as a consequence, catalyst utilization is strongly nonuniform for asymmetric regime, at variance with usual situations observed under symmetric regimes. From a control point of view, asymmetry implies the monitoring of the state of every reactor of the network, as their time history are completely different. In the reactor network here considered, symmetry breaks via frequency locking phenomena.

A detailed bifurcation analysis of the reactor network with the switch time as the bifurcation parameter is conducted. The technique used in this work allows to vary the switch time in a wide range without using limiting models. The switch time is found to affect the network asymptotic behavior. In particular, two isolae of T-periodic regimes were detected, and the observed different performances and dynamical behaviors were thoroughly characterized.

As the feed temperature is varied, hysteretic phenomena and multistability were found. At switch time values $\tau < \tau_{S3} \sim Le$ quasi-periodic regimes arising from a Neimark-Sacker bifurcation repeatedly alternate with multiperiodic regimes through frequency locking phenomena as the feed temperature is decreased. These complex regimes are found to coexist with a "simple" nonignited T-periodic regime in a wide inlet temperature range extending until the ambient temperature. This bifurcation scenario is not qualitatively affected by the heat-transfer coefficient, but rather the Neimark-Sacker bifurcation giving rise to quasi-periodic regimes shifts to lower inlet temperature values as the heat-transfer coefficient is decreased. Therefore, the stability range of symmetric T-periodic regimes becomes larger and larger when approaching adiabatic operating conditions.

At switch time values $\tau < \tau_{S3} \sim Le$ and independently from the heat-transfer coefficient, a simple hysteresis of symmetric T-periodic regimes is found as the inlet temperature is changed and complex regimes are not detected. In conclusion, it appears that the stability of the reactor network is strongly affected by variation of the switch time, the feed temperature and by the heat transfer coefficient, and this fact has to be taken into account when designing and controlling such loop of reactor.

Acknowledgments

This work was partially funded by MURST, and CNR (Gruppo Nazionale per la Difesa dai Rischi Chimico-Industriale ed Ecologici). Finally, we would like to acknowledge the reviewers for precious suggestions.

Notation

a = catalyst external surface area
c_p = heat capacity
C_A = concentration of the specie A
d_r = reactor diameter
D = mass axial dispersion coefficient
E = activation energy
$f(t)$ = forcing function
G = linear operator defined in Eq. 6
h_{fc} = heat-exchange coefficient between gas phase and catalyst
h_{fw} = heat-exchange coefficient between gas phase and reactor wall
k_0 = Arrhenius constant
k_g = gas phase axial heat conductivity
k_m = mass-transfer coefficient
k_s = solid phase axial heat conductivity
I = identity operator
L = actor length
R = gas constant
r = reaction rate
S^1 = unit circle
t^* = time
t = dimensionless time = $\nu t^*/L$
T = period
T_0 = reference temperature C
v = gas flow rate
V = volume of the reactor
y = conversion = $C_{in} - C/C_{in}$
z^* = axial coordinate
z = dimensionless axial coordinate = z^*/L
Z_3 = cyclic group

Vector and matrix

$\boldsymbol{F}$ = vector field
$\boldsymbol{x}$ = state vector
$\boldsymbol{\lambda}$ = parameter vector

Greek letters

η = effectiveness factor
ΔH = heat of reaction
θ = dimensionless temperature = $\tilde{\gamma}(T - T^0)/T^0$
ε = reactor void fraction
ε_s = catalyst porosity
ρ = density
τ = dimensionless switch time
$\Phi_{0,\tau}$ = evolution operator of the unforced system

Subscripts and superscripts

c = refers to heat exchanger
g = gas phase
h = energy balance
in = feed
m = mass
out = outlet from the system
s = solid phase
w = wall

Literature Cited

1. Kolios G, Frauhammer J, Eigenberger G. Autothermal fixed-bed reactor concepts. *Chem Eng Sci.* 2000;55:5945.
2. Matros YuSh. Unsteady process in catalytic reactor. Amsterdam: Elsevier, 1985.
3. Cotterell FG. Purifying gases and apparatus therefore. U.S. patent No.2171.733 (June 21, 1938).
4. Eigenberger G, Nieken U. Catalytic combustion with periodical flow reversal. *Chem Eng Sci*. 1988;43;2109.
5. Nieken U, Kolios G, Eigenberger G. Control of ignited steady state in autothermal fixed bed reactors for catalytic combustion. *Chem Eng Sci*. 1994;49:5507.
6. Haynes TN, Georgakis C, Caram HS. The design of reverse flow reactors for catalytic combustion system. *Chem Eng Sci.*1995;50:401.
7. Zufle H, Turek T. Catalytic combustion in a reactor with periodic flow reversal: 1. experimental results. *Chem Eng Proc*. 1997;36:327.
8. Zufle H, Turek T. Catalytic combustion in a reactor with periodic flow reversal: 2. steady state reactor model. *Chem Eng Proc*. 1997;36:341.
9. Boreskov GK, Matros Yu Sh. Unsteady-state performance of heterogeneous catalytic reactor. *Catal Revs: Sci and Eng*. 1983;25:551.
10. Matros, YuSh, Bunimovich GA. Reverse-flow operation in fixed bed catalytic reactors. *Catals Revs: Sci and Eng*. 1996;38:1.
11. Froment GF. Reverse flow operation of fixed bed catalytic reactor. In YU. Sh. Matros (Ed), Unsteady state processes in catalysis. Utrecht: VPS BV. 1990:57;152.
12. Neophytides SG, Froment GG. A bench scale study of reversed flow methanol synthesis. *Ind Eng Chem Res*. 1992;31:1583.
13. Vanden Bussche KM, Neophytides, SG, Zolotarskii IA, Froment G. Modelling and simulation of the reversed flow operation of fixed bed reactor for methanol synthesis. *Chem Eng Sci*. 1993;48:3335.
14. Matros YuSh. *Catalytic process under unsteady-state conditions*. Amsterdam: Elsevier; 1989.
15. Gerasev AP, Matros YuSh. Nonstationary method for ammonia synthesis. *Theoret. Foundation Chem Eng*. 1991;25:680.
16. Snyder JD, Subramanian S. Numerical simulation of a periodic flow reversal reactor for sulfur dioxide oxidation. Chem. Eng. Sci. 1993; 48:4051.
17. Vanden Bussche KM, Froment GF. The STAR configuration for methanol synthesis in reversed flow reactors. *Can J. Chem Eng*. 1996; 74:729.
18. Haynes TN, Caram, HS. The simulated moving bed chemical reactor. *Chem Eng Sci*. 1994;49:5465.
19. Brinkmann M, Barresi AA, Vanni M, Baldi G. Un steady state treatment of a very lean waste gases in a network of catalytic burners. *Catalysis Today*. 1999;47:263.
20. Fissore D, Barresi AA. Comparison between the reverse-flow reactor and a network of reactors for the oxidation of lean VOC mixtures. *Chem Eng Technol*. 2002;25:421.
21. Sheintuch M, Nekhamkina O. The asymptotes of loop reactors. *AICHE J*. 2005;51;224.
22. Sheintuch M, Nekhamkina O. Comparison of flow-reversal, internal-recirculation and loop reactors. *Chem Eng Sci*. 2004;59:4065.
23. Burghardt A, Berezowski M, Jacobsen EW. Approximate characteristics of a moving temperature front in a fixed-bed catalytic reactor. *Chem Eng Sci*. 1999;38:19.
24. Khinast J, Jeong YO, Luss D. Dependence of cooled reverse-flow reactor dynamics on reactor model. *AIChE J*. 1999;45:299.
25. Velardi S, Barresi AA, Manca D, Fissore D. Complex dynamic behavior of methanol synthesis in the ring reactor network. *Chem Eng Sci*. 2004;99:117.
26. Russo L, Altimari P, Mancusi E, Maffettone PL, Crescitelli S. Complex dynamics and spatiotemporal patterns in a network of three distributed chemical reactors with periodical feed switching. *Chaos, Solitons & Fractals*. 2006;3:682.
27. Kevrekidis IG, Aris R, Schmidt LD. Some common features of periodically forced reacting systems. *Chem Eng Sci*. 1986;41:1263.
28. Kevrekidis IG, Aris R, Schmidt LD. The stirred tank forced. *Chem Eng Sci*. 1986;41:1549.
29. Mancusi E, Russo L, Continillo G, Crescitelli S. Computation of frequency locking regions for a discontinuous periodically forced reactors. *Comp Chem Eng*. 2004;28:187.
30. Seydel R. *From equilibrium to chaos. Practical bifurcation and stability analysis*. New York: Elsevier; 1998.
31. Doedel E. (1997). *Lecture Notes on Numerical Analysis of Bifurcation Problems*, Hamburg, Germany; ftp.cs.condordia.ca in pub/doedel/doc/hamburg.ps.z.
32. Kuznetsov YA. *Elements of applied bifurcation theory.* 2nd ed. New York: Springer & Verlag;1998.
33. Russo L, Mancusi E, Maffettone PL, Crescitelli S. Symmetry properties and bifurcation analysis of a class of periodically forced reactors. *Chem Eng Sci*. 2002;57:5065.
34. Froment GF, Bischoff KB. Chemical Reactor Analysis and Design. New York: Wiley; 1990.
35. Reháček J, Kubíček M, Marek, M. Modelling of a tubular catalytic reactor with flow-reversal. *Chem Eng Sci*. 1992;47:2897.
36. Řeháček J, Kubíček M, Marek, M. Periodic, quasi-periodic and chaotic spatio-temporal patterns in a tubular catalytic reactor with periodic flow reversal. *Comp. Chem Eng*. 1998; 22:283.
37. Aronson DG, Golubisky M, Mallet-Paret J. Ponies on a merry-go-round in large arrays Josephson junctions. *Nonlinearity*. 1991:4;903.
38. Swift JW, Wiesenfeld K. Suppression of period doubling in symmetric systems. *Phys Rew Let*. 1984:52;705.
39. Miller W. *Symmetry groups and their applications*. New York: Academic Press; 1972.
40. Barresi AA, Vanni M, Brinkmann M, Baldi G. Control of an autothermal network of nonstationary catalytic readers. *AICHE J*. 1999; 45:1597.
41. Schreiber I, Dolník M, Choc P, Marek M. Resonance behaviour in two parameters families of periodically forced oscillators. *Physics Letts A*. 1988;128:66.
42. Russo L, Mancusi E, Maffettone PL, Crescitelli S. Non-linear analysis of a network of 3 continuous stirred tank reactors with periodic feed switching: symmetry and symmetry-breaking. *Int J Biff and Chaos*. 2004;14:1325.
43. Nikolaev EV, Shnol EE. Bifurcations of cycles in systems of differential equations with a finite symmetry group I. *J Dynam. and Control Syst*. 1998;4:315.
44. Nikolaev EV, Shnol EE. Bifurcations of cycles in systems of differential equations with a finite symmetry group - II. *J Dynam and Control Syst*. 1998;4; 343.
45. Khinast J, Gurumoorthy A, Luss D. Complex dynamic features of a cooled reverse-flow reactor. *AIChE J*. 1998:44;1128.

Manuscript received Aug. 4, 2005, and revision received Mar. 8, 2006.